

## Analyzing powers in $\pi^{\pm}p$ elastic scattering from $T_{\pi} = 98$ to 263 MeV

M. E. Sevier, A. Feltham, and P. Weber

*University of British Columbia, Vancouver, British Columbia, Canada V6T 1W5*

G. R. Smith, D. R. Gill, D. Healey, D. Ottewell, and G. D. Wait

*TRIUMF, Vancouver, British Columbia, Canada V6T 2A3*

J. T. Brack, M. Kohler, J. J. Kraushaar, D. Oakley, R. J. Peterson, and R. A. Ristinen

*University of Colorado, Boulder, Colorado 80309*

E. L. Mathie

*University of Regina, Regina, Saskatchewan, Canada S4S 0A2*

N. R. Stevenson and R. B. Schubank

*University of Saskatchewan, Saskatoon, Saskatchewan, Canada S7N 0W0*

E. Gibson

*California State University, Sacramento, California 95819*

R. Arndt

*Virginia Polytechnic Institute and State University, Blacksburg, Virginia 24061*

(Received 18 May 1989)

Angular distributions of the analyzing powers for  $\pi^+p$  and  $\pi^-p$  elastic scattering have been measured in a single-scattering experiment employing a polarized proton target. Measurements were obtained for pion energies of 98, 139, 166, 215, and 263 MeV. The addition of these data to the existing  $\pi p$  database significantly reduces the uncertainties in all  $S$  and  $P$  phase shifts for  $\pi p$  reactions over the delta resonance.

### I. INTRODUCTION

Pion-nucleon elastic scattering is the simplest and most fundamental process involving pions in intermediate energy physics, yet many of the phase shifts describing  $\pi^{\pm}p$  scattering have large uncertainties. This situation can be traced in part to the paucity of precision spin-dependent data for these reactions. Spin-dependent data, such as analyzing powers, are sensitive to interference between amplitudes so that smaller, nonresonant partial waves can be as important as the resonant  $P_{33}$  partial wave which dominates the differential and total cross sections.

Recently, there has been renewed interest<sup>1</sup> in the  $\pi N$  system due to the connection between  $\pi N$  observables and the  $\sigma$  term. The  $\sigma$  term can be related to the strange quark content of the proton via chiral perturbation theory. The  $\pi N$  observables can be related to the  $\sigma$  term via the  $s$ -wave scattering length  $a_0^+$ . Although this connection occurs at the unphysical (negative energy) Cheng-Dashen point, it is important to have precise knowledge of the phase shifts at higher energies in order to make a more accurate extrapolation to the unphysical region. Quite apart from their usefulness in contributing to our understanding of the  $\sigma$  term, new  $\pi p$  analyzing power data, and the resulting improvement in our knowledge of the partial-wave amplitudes, are fundamen-

tally important to our understanding of pion interactions with nuclei. These amplitudes form the input to microscopic theories which deal with pion-nuclear  $\pi A$  interactions, as well as nucleon-nucleus interactions.

Recent measurements<sup>2,3</sup> of the  $\pi^{\pm}p$  differential cross section at low energies lie as much as 20% below the presently accepted phase-shift solutions. This astonishing discrepancy is the focus of many current  $\pi N$  experiments. Although the present experiment was performed primarily at energies above the region where the largest discrepancies are found, improvement in our knowledge of the partial waves in the energy region of this experiment has a bearing on the low-energy phase-shift solutions by virtue of dispersion relations which connect the two energy regions. For these reasons, the data presented in this paper should contribute to our understanding of the issues already mentioned.

For  $\pi^+p$  elastic scattering there are only three reasonably complete angular distributions of analyzing power measurements below 263 MeV, one at 236 MeV (Ref. 4) and those at 166 and 194 MeV.<sup>5</sup> There is a four-angle measurement at 95 MeV and there are single-angle measurements<sup>5</sup> at 176 and 185 MeV. For  $\pi^-p$  scattering, there are only two analyzing power measurements below 263 MeV, one at 98.0 MeV (four angles) and the other at 238 MeV,<sup>6</sup> although some older data<sup>7</sup> exist at 229 and

250 MeV. The uncertainties associated with many of these data are large, especially for  $\pi^-\bar{p}$ .

With the development of techniques to measure spin observables of the  $\pi\bar{d}$  elastic scattering reaction,<sup>8-10</sup> a complete set of analyzing power data for both  $\pi^+\bar{p}$  and  $\pi^-\bar{p}$  can be obtained relatively simply and quickly. This investigation used these techniques with the aim of providing a definitive systematic data set for  $\pi^+\bar{p}$  and  $\pi^-\bar{p}$  elastic scattering over the delta resonance. The experiment was carried out on the M11 pion channel at TRIUMF. Data were gathered simultaneously at six pion scattering angles using six pion counter telescopes and six recoil proton counters. The polarized proton target was developed at TRIUMF. It included a  $^3\text{He}$ - $^4\text{He}$  dilution refrigerator and a superconducting split-pair magnet.

With a target polarized normal to the scattering plane, the analyzing power  $A(\theta)$  is, according to the Madison convention,

$$A(\theta) = \frac{\sigma^+ - \sigma^-}{\sigma^+ P^- + \sigma^- P^+ - (P^+ + P^-)\sigma^b},$$

where  $\sigma^+$  and  $\sigma^-$  refer to the measured differential cross sections with spin direction (+) and spin direction (-), respectively. The (+) direction is defined by the cross product of the incoming and outgoing pion momenta. The positive direction thus defined pointed downward in the laboratory reference frame. The direction of polarization is positive along the target magnetic field.  $P^+$  and  $P^-$  refer to the target polarization in the positive and negative directions, respectively. The measured background differential cross section is  $\sigma^b$ , which is unpolarized and therefore independent of the direction of target polarization.

## II. POLARIZED TARGET

The polarized target consisted of 2.4 cc of frozen 1-mm diameter beads contained in a thin walled teflon basket measuring 22 mm  $\times$  18 mm  $\times$  6 mm. The beads were composed of a mixture of *N*-butyl alcohol ( $\text{C}_4\text{H}_9\text{OH}$ ) and 5%  $\text{H}_2\text{O}$  into which EHBA- $\text{C}^{10}$  (Ref. 11) was dissolved to a density of  $6 \times 10^{19}$  molecules/ml. The packing fraction of the butanol beads was approximately 0.7. The teflon basket, which also served as a support for an NMR pickup coil, was immersed in a mixture of  $^3\text{He}$ - $^4\text{He}$  in the mixing chamber of a dilution refrigerator.

Microwaves used for the dynamic polarization of the target were provided by a 100 mW impact avalanche transit-time (IMPATT) tunnel diode source capable of delivering frequencies between 69 and 72 GHz. As the target polarization increased, the microwave power to the target microwave cavity was gradually lowered from 2 to 0.25 mW. The frequency delivered was stabilized by computer feedback to a tolerance of 1 MHz. The positive polarization state was achieved by applying microwaves at 70.450 GHz and the negative state with 70.870 GHz. This frequency change was the only experimental parameter varied from one polarization to the other.

The polarizing field of 2.55 T was provided by two superconducting coils in a Helmholtz configuration with a vertical magnetic field axis. The data were acquired with

the target in the frozen spin mode at a holding field of 1.25 T. The magnitude of the polarization achieved varied from run to run but was typically 75% for the negative state and 65% for the positive state.

The magnitude of target polarization was determined from measurements of the proton NMR signal. The NMR pickup coil consisted of a 7 turn coil of 0.1-mm diameter copper wire which surrounded the target material. A circuit design was used which removed all active electronics from the refrigerator. The rf NMR signals were measured at the end of a  $3\lambda/2$  cable. The  $Q$  curve was canceled with an equivalent tuned circuit at room temperature. The real part of the NMR signal was measured using a synchronous detector.

The target polarization was obtained from analysis of the NMR signals using the thermal equilibrium (TE) technique. The TE technique involves comparing the total area of the dynamically polarized proton NMR signal with the total area of the TE NMR signal. The TE polarization can be deduced from the known values of temperature and magnetic field, assuming a Maxwell-Boltzmann distribution, according to

$$P(\text{TE}) = \tanh \left[ \frac{\mu B}{kT} \right] \approx \frac{\mu B}{kT},$$

where  $\mu$  is the proton magnetic moment,  $B$  is the magnetic field,  $k$  is Boltzmann's constant, and  $T$  is the temperature. For values of  $B = 2.5506$  T and  $T = 1$  K, the TE polarization was 0.002 606. The temperature of the target was obtained by averaging the readings of two calibrated resistors in the mixing chamber of the dilution refrigerator. The temperature calibrations of the thermometers were made by comparison with  $^3\text{He}$  and  $^4\text{He}$  vapor pressure measurements to an accuracy of 1%. The dilution temperature was capable of reaching temperatures of approximately 100 mK. During the microwave bombardment, however, the temperature of the target rose to approximately 0.3 K. The magnitude of the magnetic field was measured by utilizing the more conventional aspects of the proton NMR signal, namely that the NMR central frequency is proportional to the magnetic field strength. In practice, the current in the polarizing magnet was adjusted until the proton NMR signal frequency was centered at  $108.600 \pm 0.002$  MHz. This frequency corresponds to a magnetic field of  $2.5506 \pm 0.0003$  T.

Once the magnitude of the TE polarization was calculated, the magnitude of dynamic polarization was obtained from the ratio of the integrated areas of the dynamic and TE NMR signals. The determination of the NMR background was made by averaging the measured background on both sides of the NMR signal. This procedure was performed the same way for both the dynamic and the TE NMR signals. Finally the background under the proton NMR signal was determined by a linear fit to the background on either side of the NMR signal. The NMR signal intensity was measured as the NMR frequency was swept between 108.344 and 108.856 MHz, i.e., over a frequency range of 512 kHz in 256 two kHz steps. In order to estimate the NMR background in this region, one requires measurements just below and just

above these limits in order to avoid the region sensitive to proton spin flips. In principle one could merely sweep the NMR frequency in regions just below 108.344 MHz and just above 108.856 MHz. However, the NMR circuit is highly tuned and in practice it is quite difficult to select precisely all of the tuning parameters (such as the cable length, the tuned circuit and the NMR center frequency, and the phases of the RF signals to the synchronous detector). Therefore, instead of varying the NMR frequency interval, the proton NMR signal was swept out of this frequency interval by slightly adjusting the magnetic field of the target. For this experiment, the NMR background was obtained by averaging measurements obtained at magnetic field strengths 1% above and 1% below the nominal 2.55-T value. The uncertainty in the integrated area of the TE NMR signal resulting from this procedure was determined by the standard deviation of the measured values obtained at intervals during the course of the experiment. The final value was the average of four sets of ten TE measurements.

### III. EXPERIMENTAL PROCEDURE

The detection system used for the measurements is shown in Fig. 1. The main characteristics of the detection system are as follows: A solid angle of 27 msr for each of six independent arms ( $i=1,6$ ) was defined by a scintillator ( $\pi 2_i$ ) of dimensions 9.0 cm  $\times$  30.0 cm located 1 m from the polarized target. Together with another

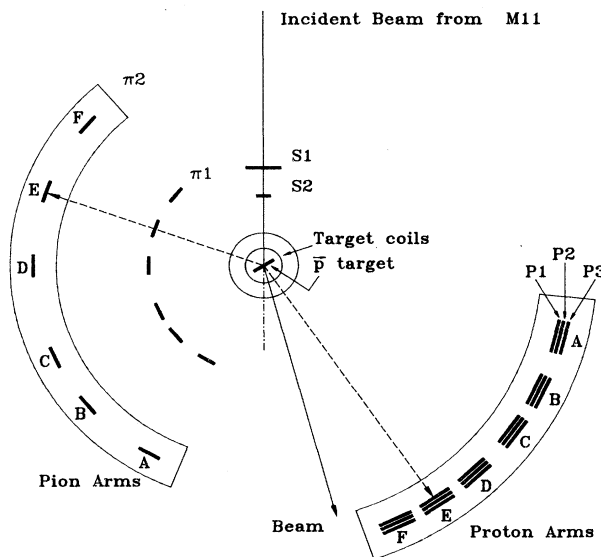


FIG. 1. The experimental arrangement. The incident beam passes through the two scintillators S1 and S2 before striking the target. The beam is bent by the magnetic holding field of the polarized target but the combined effect of the central field and return field of the superconducting solenoid is to direct any particle initially aimed at the center of the target onto the center of the target. Six counter arms used to detect the pions and protons so that data are acquired simultaneously at six pion scattering angles. The scintillator thicknesses are not to scale.

scintillator ( $\pi 1_i$ ) at 0.5-m radius with dimensions 9.0 cm  $\times$  16.5 cm, this constituted one of six pion telescopes. Each of the scintillators in the pion telescopes was 3.2-mm thick.

Each pion telescope was placed in coincidence with an associated recoil proton arm consisting of three scintillators. The first scintillator ( $P1_i$ ) at a radius of 1.3 m from the target was a thin (3.2-mm) scintillator of dimensions 9.0 cm  $\times$  40.0 cm which provided time-of-flight (TOF) as well as energy loss ( $\Delta E$ ) information. Following this counter were two further scintillators ( $P2_i$ ,  $P3_i$ ) of dimensions 9.0 cm  $\times$  41.0 cm and thicknesses 1.27 and 0.64 cm, respectively. These scintillators were available for further energy-loss information, but were found not to be needed. A more detailed description of the experimental setup can be found in Refs. 9 and 10.

The flux of the incident beam was counted directly with scintillators S1 and S2 in coincidence, each of which was 1.6-mm thick. The size of S2 was chosen such that its image at the target would be smaller than the target. The intensity of protons in the incident positive pion beam was reduced by using a differential degrader near the midplane of the M11 channel. Those protons remaining in the beam were eliminated by placing pulse-height requirements ( $\overline{S2}$ ) on S2 in the beam scaler and in the event trigger, so that pions were accepted but protons of similar momentum were not. The event trigger was defined as

$$S1 \cdot S2 \cdot \overline{S2} \cdot \pi 1_i \cdot \pi 2_i \cdot P1_i .$$

Pions were distinguished from contaminant electrons and muons by the cyclotron rf referenced TOF to S2. The incident pion flux was typically 2 MHz for  $\pi^+$ , although this rate fell to 0.6 MHz for runs at 263 MeV. For the  $\pi^-$  measurements, the incident beam rate was typically 1 MHz, except at 263 MeV where the rate was 0.3 MHz. The position of the target within its cryostat was verified by exposing photographic film placed downstream of the target to the beam from M11. The horizontal divergence of the beam was less than  $1^\circ$ . The vertical divergence of the beam was also constrained to be less than  $1^\circ$  by the vertical dimension of the in-beam scintillator S2. The incident beam energies in this experiment were  $98.0 \pm 0.5$ ,  $138.8 \pm 0.5$ ,  $166.0 \pm 0.5$ ,  $214.6 \pm 0.5$ , and  $263.0 \pm 0.5$  MeV for both the  $\pi^+$  and  $\pi^-$  measurements. These energies and uncertainties are based on the established<sup>12</sup> calibration procedure for the M11 channel. The quoted energies are the mean values at the center of the polarized target and take into account energy loss through the S1 and S2 scintillators, air, polarized target material, and surrounding heat shield. The momentum acceptance of the M11 channel for the  $\pi^- p$  runs corresponding to each of these bombarding energies was, respectively,  $\Delta p/p = \pm 1.1$ ,  $\pm 0.9$ ,  $\pm 0.6$ ,  $\pm 1.1$ , and  $\pm 1.1\%$ . The  $\pi^+ p$  measurements were all made with a momentum acceptance of  $\pm 0.25\%$ .

The magnetic field at the target was held at 2.5 T while polarizing and was lowered to 1.25 T for data taking. This reduced the effect of the magnetic field on the particle trajectories and enabled a larger angular range to be measured. It is important to note that the direction of

the magnetic field at the target was the same for  $P^+$  and  $P^-$ , hence the particle trajectories were not affected by a polarization change. Generally two data runs were made in a particular state before the polarization was reversed and six data runs were taken for each angle and energy set. A typical data taking sequence would be +(change energy)+ - - + + - (change energy)-, etc. Taking data in this sequence enables potential systematic uncertainties to be more easily identified. The polarization was measured before and after each set of two runs with the same polarization. The polarization decay rate was determined for each polarization state; it was typically 0.0035/h, runs were 2 h long, and the time between polarization measurements was 4-5 h. This information was used to determine the average target polarization for each run.

The influence of the polarizing magnetic field of the target on the particle trajectories was determined by means of a ray tracing computer code. This code was used to determine the laboratory angles for the two detector arms corresponding to the appropriate  $\pi p$  elastic scattering kinematics. The angular range accessible to measurement was limited by the requirement of our experimental technique that the recoil proton be detected in coincidence with the scattered pion. Consequently the most forward pion angle measured at energies below 215 MeV was where the recoil proton had just enough energy to escape the target and reach the P1 scintillator. At 215 and 263 MeV the angular range was limited by the physical dimensions of the support table for the scintillator telescopes.

Final analysis of the data was performed by constructing software polygons around the  $\pi p$  elastic events identified in two-dimensional histograms of the proton TOF vs the proton energy loss in the P1 scintillator. A typical two-dimensional histogram with such a polygon is shown in Fig. 2. In addition, software filters were placed on the pion TOF and energy loss in the  $\pi 2$  scintillator to select elastically scattered pions in the  $\pi$  arm. The resulting scatterplot provides particle identification and clearly

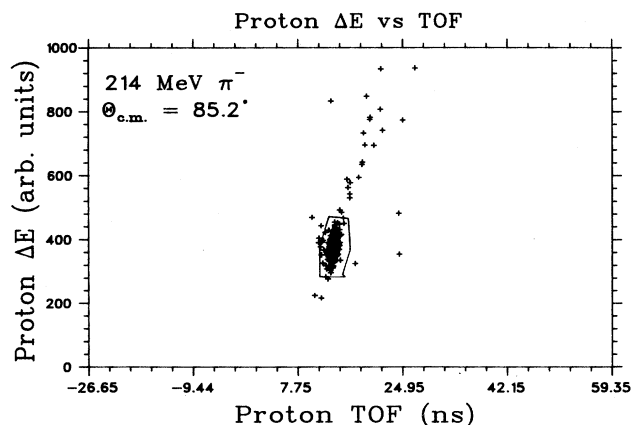


FIG. 2. A typical two-dimensional plot of the proton TOF vs the proton energy loss in P1. Events inside the polygon were taken to be  $\pi p$  elastic scattering events.

distinguishes  $\pi p$  elastic events from other processes. Typical foreground and background histograms of the difference between scattered proton TOF and scattered pion TOF from target to detector are shown in Fig. 3. These are raw histograms with no software filters.

Measurements were made of the background arising from quasielastic  $\pi p$  scattering from the contaminant carbon, oxygen, and helium nuclei in the polarized target and coolant. To achieve this, the butanol bead target was replaced with graphite granules of similar dimensions. However, because pure graphite has a different density than that of frozen butanol, the background target had twice the effective target thickness of carbon. The main source of background was expected to be the target coolant which was a mixture of liquid  $^3\text{He}$  and  $^4\text{He}$  and which provides about 5 times as many scatterers as the carbon and oxygen in the butanol. The normalization of the background yield therefore depends on the relative cross sections for quasifree  $\pi p$  elastic scattering on carbon and helium.

To determine the relative normalization of the background yield we compared the number of counts in the region away from the two-body kinematic peak with the foreground target to the number with the background target. The comparison showed an equal number of

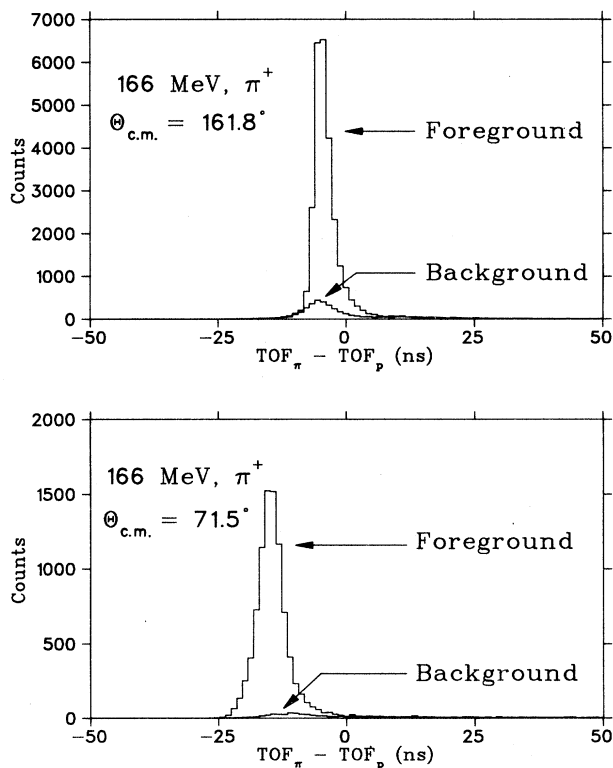


FIG. 3. Typical raw spectra of the difference between pion TOF and proton TOF for foreground and background runs at two different angles. These data were obtained for  $\pi^+p$  elastic scattering at 166 MeV. Note that the background at the backward angle is much larger than at the forward angle.

counts per unit beam even though there were twice as many carbon nuclei in the background target. This showed that the dominant source of background was indeed the helium nuclei of the target coolant. Further evidence that the background is predominantly due to the target coolant can be found in the work of Brack *et al.*<sup>2</sup> In that experiment, absolute differential cross sections for  $\pi p$  elastic scattering were measured with essentially the same detection apparatus as in this work, but with a solid  $\text{CH}_2$  (polyethylene) target. They found that the background due to the carbon of their target was typically about a factor of 10 smaller than our measured backgrounds. Since the present experiment also used a target that basically consists of carbon and hydrogen, our much larger background can be attributed to the helium of the target coolant. The number of scatterers was taken to be the same for the foreground and the background. These background measurements were made at the end of the experiment running period, for each of the angles and energies and magnetic fields at which foreground data were acquired.

Many of the experimental uncertainties associated with differential cross-section measurements, such as the target thickness, solid angle, and counter efficiencies, cancel out in the expression for  $A(\theta)$  and therefore do not contribute to the uncertainties in the present experiment. It was observed that the size of the background varied from

around 1% of the foreground at forward angles to around 15% at backward angles. Changing the background normalization by even a factor of 1.5 gives rise to a maximum shift of only 0.01 in  $A(\theta)$ . The impact of a background renormalization by up to a factor of 1.5 was less than the quoted uncertainty in  $A(\theta)$  for every angle and energy studied in this experiment. The polarizations used in the above expression were the values averaged over each run as described earlier.

The uncertainty in the measured analyzing power was determined by forming the quadratic sum of the uncertainties in each of the above quantities weighted by the partial derivative of  $A$  with respect to each quantity, i.e.,

$$\begin{aligned} \Delta A^2 = & (\Delta\sigma^+)^2 \left[ \frac{\partial A}{\partial \sigma^+} \right]^2 + (\Delta\sigma^-)^2 \left[ \frac{\partial A}{\partial \sigma^-} \right]^2 \\ & + (\Delta\sigma^b)^2 \left[ \frac{\partial A}{\partial \sigma^b} \right]^2 \\ & + \frac{1}{16} (\Delta P^+ + \Delta P^-)^2 \left[ \frac{\partial A}{\partial P^+} + \frac{\partial A}{\partial P^-} \right]^2. \end{aligned}$$

The uncertainties  $\Delta\sigma^\pm$  and  $\Delta\sigma^b$  were the statistical uncertainties. The uncertainties in  $P^+$  and  $P^-$  were highly correlated as they were based on the same normalization as discussed above. For that reason the individual contri-

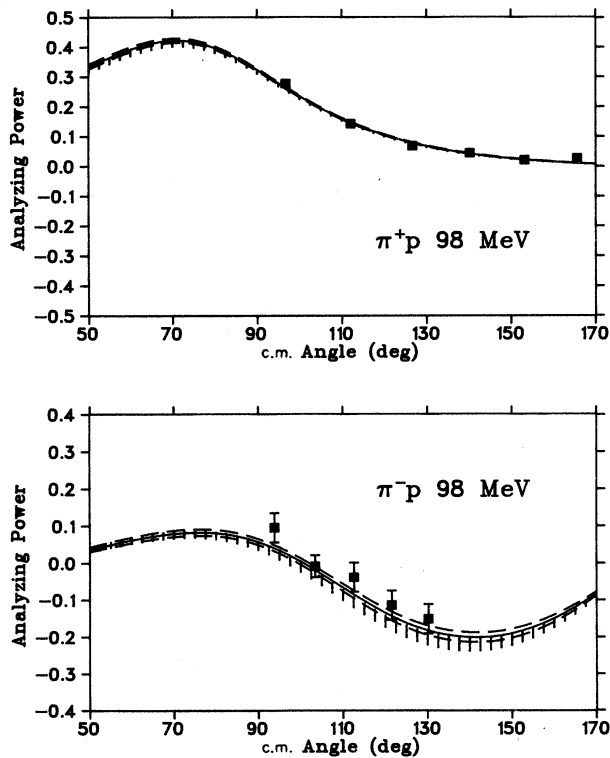


FIG. 4. Analyzing powers for  $\pi^+ p$  and  $\pi^- p$  elastic scattering at 98 MeV. The vertical lines show the range of values predicted by the old phase-shift solution. The solid curves are from the new solution. The dashed curves bracketing the solid curves show the uncertainty of the new solution.

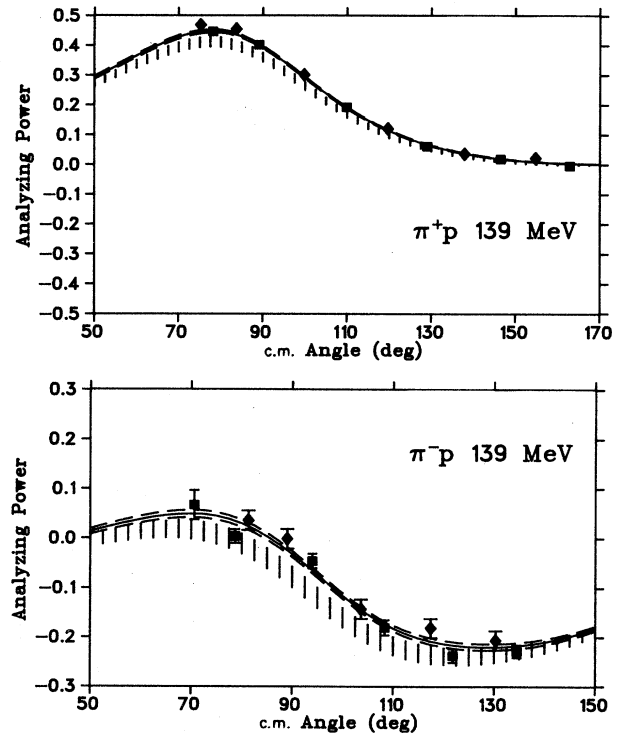


FIG. 5. Analyzing powers for  $\pi^+ p$  and  $\pi^- p$  elastic scattering at 139 MeV. The vertical lines show the range of values predicted by the old phase-shift solution. The solid curves are from the new solution. The dashed curves bracketing the solid curves show the uncertainties of the new solution. The diamond and square data points are for two different sets of angles for the six pion detectors.

butions to the total uncertainty due to  $P^+$  and  $P^-$  were averaged and then included in the quadratic sum. The uncertainty in the magnitude of the target polarization was 1.6%. The typical statistical uncertainty in the relative differential cross sections varied from 0.4% for  $\pi^+p$  at 166 MeV to 4% for  $\pi^-p$  at 98 MeV. The statistical uncertainty in the background measurement varied from 1 to 10%.

#### IV. RESULTS

The measured analyzing powers are displayed in Figs. 4–8 and listed in Table I. The uncertainties quoted in the table and shown in the figures are the combined systematic and statistical errors as described earlier. The diamond and square data points shown in Figs. 5–8 refer to the two sets of angular settings for the six detectors that were used.

There were only two energies at which the measured analyzing power data could be directly compared with the results of others, i.e.,  $\pi^-p$  at 98 MeV (Ref. 6) and  $\pi^+p$  at 166 MeV.<sup>5</sup> This comparison is shown in Fig. 9. It can be seen that the present measurements are in general agreement with the earlier measurements except around 90° for  $\pi^+p$  at 166 MeV. It is also evident that the uncertainties of the present measurements are far smaller than those of the earlier measurements. The general level of agreement of the new data with the older data can be inferred from the predictions of the “old” phase-shift solutions. These are displayed in Figs. 4–8 as vertical bars which cover the range of possible values for the analyzing powers and so reflect the uncertainties of the earlier data.

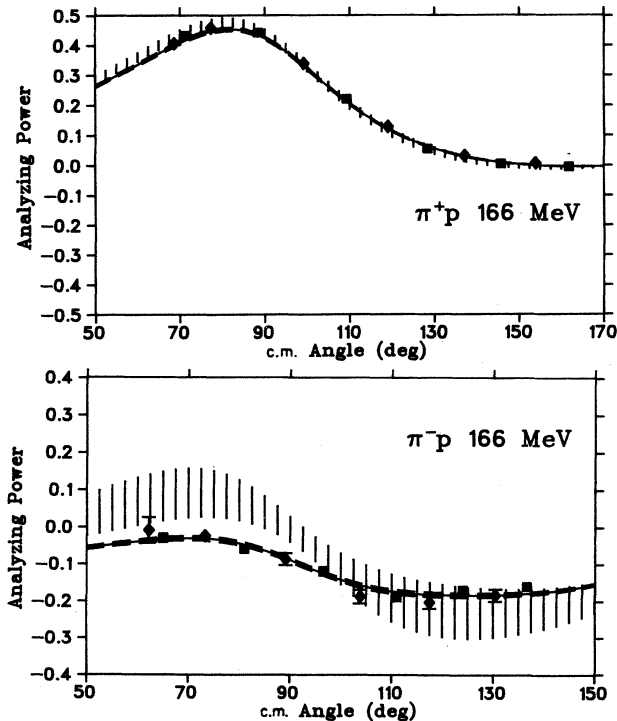


FIG. 6. Analyzing powers for  $\pi^+p$  and  $\pi^-p$  elastic scattering at 166 MeV. The other details are as in Fig. 5.

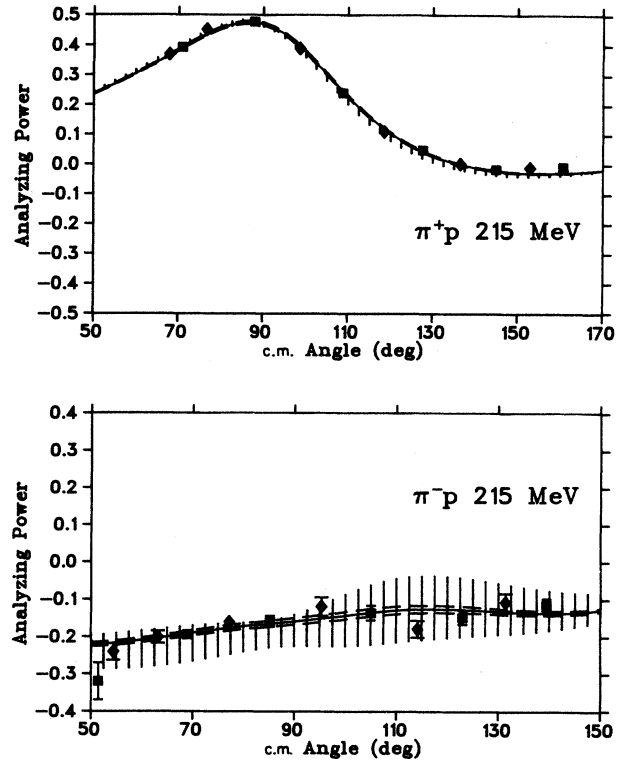


FIG. 7. Analyzing powers for  $\pi^+p$  and  $\pi^-p$  elastic scattering at 215 MeV. The other details are as in Fig. 5.

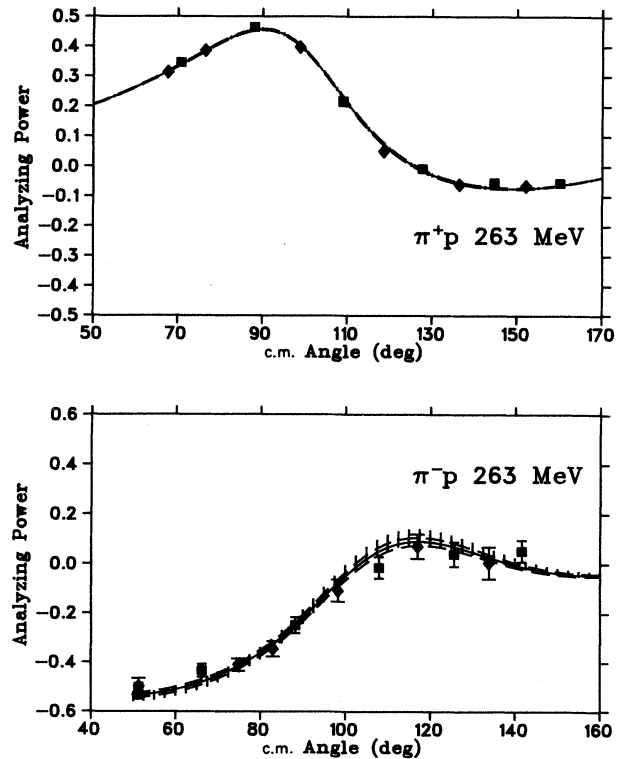


FIG. 8. Analyzing powers for  $\pi^+p$  and  $\pi^-p$  elastic scattering at 263 MeV. The other details are as in Fig. 5.

TABLE I. Measured analyzing powers for  $\pi^\pm p$  elastic scattering.

$T_\pi$ (lab) (MeV)	$\theta_{c.m.}$ (deg)	$\pi^+ p$		$\pi^- p$	
		$A(\theta)$	$\theta_{c.m.}$ (deg)	$A(\theta)$	$\theta_{c.m.}$ (deg)
98	96.7	0.277±0.012	93.8	0.10±0.04	
	112.1	0.142±0.009	103.4	-0.01±0.03	
	126.6	0.068±0.007	112.6	-0.04±0.04	
	140.2	0.044±0.006	121.5	-0.12±0.04	
	153.2	0.020±0.006	130.2	-0.15±0.04	
	165.6	0.026±0.012			
139	75.2	0.468±0.011	70.6	0.07±0.03	
	78.1	0.446±0.009	78.7	0.003±0.014	
	83.7	0.45±0.01	81.3	0.04±0.02	
	89.1	0.401±0.008	89.0	-0.00±0.02	
	99.8	0.300±0.008	94.0	-0.047±0.015	
	109.9	0.191±0.006	103.6	-0.14±0.02	
	119.7	0.119±0.006	108.3	-0.181±0.016	
	129.0	0.060±0.005	117.4	-0.18±0.02	
	137.9	0.035±0.005	121.8	-0.238±0.014	
	146.5	0.018±0.004	130.3	-0.21±0.02	
	154.8	0.021±0.005	134.5	-0.229±0.013	
	162.9	-0.005±0.006			
	166	68.6	0.406±0.009	62.2	-0.01±0.04
71.5		0.433±0.009	65.0	-0.030±0.012	
77.3		0.458±0.009	73.3	-0.024±0.015	
88.4		0.443±0.009	81.0	-0.06±0.01	
99.1		0.339±0.008	89.1	-0.087±0.017	
109.3		0.220±0.007	96.5	-0.120±0.012	
119.0		0.128±0.006	103.8	-0.188±0.019	
128.3		0.054±0.005	111.0	-0.19±0.01	
137.1		0.031±0.005	117.5	-0.204±0.017	
145.7		0.004±0.005	124.0	-0.170±0.011	
153.9		0.006±0.005	130.4	-0.184±0.017	
161.8		-0.006±0.006	136.6	-0.16±0.01	
215		67.8	0.370±0.008	51.4	-0.32±0.05
	70.8	0.393±0.008	54.4	-0.24±0.02	
	76.6	0.452±0.009	63.2	-0.20±0.02	
	87.9	0.478±0.009	68.9	-0.194±0.011	
	98.6	0.390±0.01	77.2	-0.161±0.016	
	108.8	0.240±0.009	85.2	-0.159±0.015	
	118.5	0.11±0.01	95.3	-0.12±0.02	
	127.7	0.048±0.007	105.0	-0.14±0.02	
	136.5	0.002±0.008	114.2	-0.18±0.02	
	144.9	-0.016±0.007	123.0	-0.148±0.019	
	152.9	-0.010±0.009	131.4	-0.11±0.02	
	160.7	-0.007±0.007	139.4	-0.113±0.016	
	263	67.6	0.313±0.007	51.3	-0.52±0.03
70.7		0.346±0.008	51.3	-0.50±0.03	
76.5		0.386±0.008	66.2	-0.43±0.03	
88.0		0.464±0.012	74.8	-0.41±0.03	
98.8		0.397±0.011	83.0	-0.35±0.03	
109.0		0.215±0.015	88.2	-0.25±0.03	
118.6		0.049±0.011	98.3	-0.11±0.05	
127.7		-0.009±0.012	107.9	-0.02±0.04	
136.4		-0.06±0.01	117.0	0.07±0.05	
144.6		-0.055±0.012	125.6	0.04±0.05	
152.1	-0.07±0.01	133.8	0.00±0.06		
160.1	-0.056±0.012	141.6	0.05±0.04		

The effects of the newly measured analyzing powers on the phase-shift analyses are given in Table II and in Figs. 4–8. These were determined by means of the program SAID.<sup>13</sup> Single-energy analyses were first performed at five energies from 100 to 250 MeV on data excluding the new measurements. The *S*- and *P*-wave phase shifts derived from these fits are given in Table II as the old solution. Our data were then included in the data base and the analyses repeated with the results given in Table II as the “new” solution. Figures 4–8 illustrate predictions of analyzing powers with the new solutions as the solid line, with the dashed banding to indicate the uncertainties.

Inclusion of the new data leads to a considerable reduction in the errors on the analyzing power predictions in most cases, but it is most pronounced for  $\pi^- p$  at 139, 166, and 215 MeV where our data lead to a factor of 10–20 reduction in the uncertainties. This can be traced to the paucity of spin-dependent data for the reactions in the region of the delta resonance. Although there are quite extensive data for differential cross sections in this energy region, these data provide sensitivity mainly to the dominant  $P_{33}$  partial wave of the delta resonance. Consequently, the other partial waves that contribute to  $\pi p$  elastic scattering at resonance energies have not been satisfactorily determined until now. The analyzing powers

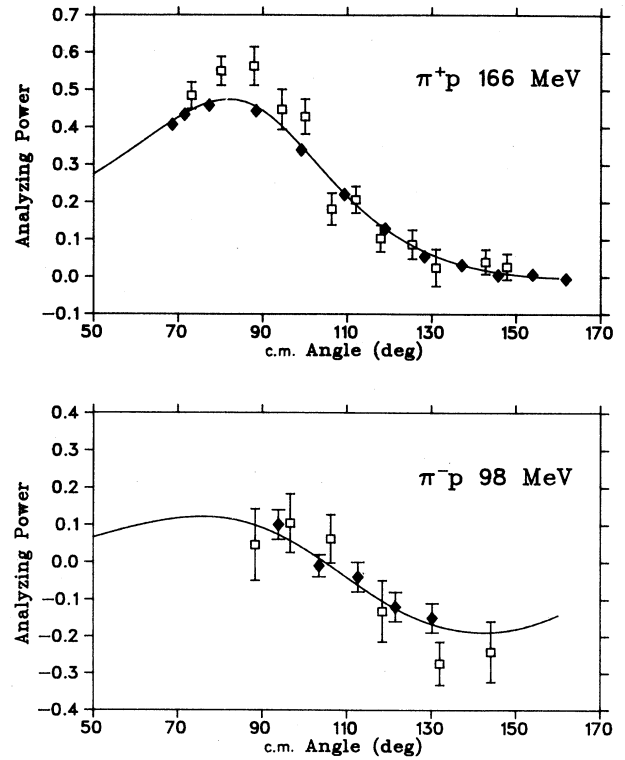


FIG. 9. Comparison of the present measurement (diamonds) with the  $\pi^- p$  data of Alder *et al.* (Ref. 6) at 98 MeV (open squares) and the  $\pi^+ p$  data of Amsler *et al.* (Ref. 5) at 166 MeV (open squares). The solid curves are the predictions calculated with SAID (Ref. 13) using the SM88 phase-shift solution.

TABLE II. Phase shifts in degrees for  $\pi^\pm p$  elastic scattering.

$T_\pi$ MeV	Partial wave	Old solution	New solution
100	$S_{11}$	$8.59 \pm 0.16$	$8.69 \pm 0.15$
	$S_{31}$	$-8.65 \pm 0.17$	$-8.87 \pm 0.13$
	$P_{11}$	$-0.89 \pm 0.13$	$-0.82 \pm 0.12$
	$P_{13}$	$-1.70 \pm 0.10$	$-1.61 \pm 0.09$
	$P_{31}$	$-1.97 \pm 0.10$	$-2.00 \pm 0.09$
	$P_{33}$	$22.29 \pm 0.06$	$22.23 \pm 0.06$
125	$S_{11}$	$8.76 \pm 0.20$	$8.84 \pm 0.15$
	$S_{31}$	$-9.4 \pm 0.5$	$-10.43 \pm 0.14$
	$P_{11}$	$-0.7 \pm 0.2$	$-0.81 \pm 0.12$
	$P_{13}$	$-2.18 \pm 0.16$	$-2.11 \pm 0.13$
	$P_{31}$	$-2.84 \pm 0.18$	$-2.90 \pm 0.10$
	$P_{33}$	$37.14 \pm 0.10$	$36.95 \pm 0.06$
175	$S_{11}$	$9.2 \pm 0.4$	$10.02 \pm 0.18$
	$S_{31}$	$-13.9 \pm 0.5$	$-13.36 \pm 0.18$
	$P_{11}$	$-0.1 \pm 1.2$	$1.12 \pm 0.11$
	$P_{13}$	$-1.2 \pm 0.5$	$-1.1 \pm 0.4$
	$P_{31}$	$-4.9 \pm 0.5$	$-4.30 \pm 0.12$
	$P_{33}$	$78.2 \pm 0.2$	$78.30 \pm 0.16$
200	$S_{11}$	$10.8 \pm 0.6$	$10.58 \pm 0.14$
	$S_{31}$	$-15.3 \pm 0.4$	$-15.5 \pm 0.2$
	$P_{11}$	$2.9 \pm 1.2$	$2.42 \pm 0.14$
	$P_{13}$	$-2.3 \pm 0.6$	$-2.3 \pm 0.5$
	$P_{31}$	$-5.6 \pm 0.4$	$-5.23 \pm 0.14$
	$P_{33}$	$97.6 \pm 0.3$	$97.5 \pm 0.3$
250	$S_{11}$	$10.9 \pm 0.4$	$11.0 \pm 0.2$
	$S_{31}$	$-18.17 \pm 0.19$	$-18.19 \pm 0.18$
	$P_{11}$	$7.8 \pm 0.3$	$7.6 \pm 0.2$
	$P_{13}$	$-2.46 \pm 0.17$	$-2.54 \pm 0.16$
	$P_{31}$	$-6.7 \pm 0.3$	$-7.00 \pm 0.16$
	$P_{33}$	$121.57 \pm 0.12$	$121.60 \pm 0.11$

for the  $\pi^- p$  reaction are particularly sensitive to the isospin  $\frac{1}{2}$  partial waves, while the differential cross sections in this energy region are sensitive primarily to the  $T = \frac{3}{2}$  partial waves. Therefore the analyzing powers for this reaction predicted by a partial-wave analysis were quite uncertain at 139, 166, and 215 MeV, i.e., in the region of the delta resonance.

It is worth noting that where the uncertainties in the predictions for the analyzing powers from the old solutions are small, such as for 263 MeV  $\pi^+ p$ , our data are in excellent agreement with those calculations. Such consistency lends support both to the existing data base at these energies and to the accuracy attained in this experiment.

The general effect of the new data on the phase shifts is a substantial reduction of uncertainties, rather than a change of values. The major exception is the  $P_{11}$  phase shift at 175 MeV, where the old solution gives  $-0.1^\circ \pm 1.2^\circ$  and the new solution gives  $1.1^\circ \pm 0.1^\circ$ . The exact energy dependence of this phase shift is particularly important because pion absorption through the  $P_{11}$  channel has been identified as a major source of uncertainty in Faddeev calculations of spin observables for  $\pi d$  elastic scattering.<sup>9,10,14</sup> The other appreciable effects of our data are on the  $S_{11}$ ,  $S_{31}$ , and  $P_{31}$  partial waves. The uncertainties for these partial waves are reduced by factors of between 2 and 5. Our analyzing power data have been included in the data base used for SM88.<sup>13</sup>

Differential cross sections were calculated for  $\pi^- p$  and  $\pi^+ p$  at 125 and 200 MeV using the program SAID (Ref. 13) to determine what differences could be found between the predictions from the old and new phase-shift solutions listed in Table II. The differences in the differential cross sections were found to be exceedingly small; they were a maximum of 1.6% for  $\pi^-$  at 125 MeV.

It is clear that measurements of the analyzing powers at pion energies below 98 MeV would be useful, since no data are available in that energy region. The technique used in the present experiment cannot be readily employed for such measurements since the recoil proton would have too low an energy to reach the proton counter.

#### ACKNOWLEDGMENTS

It is our pleasure to acknowledge the support and assistance of the TRIUMF staff and particularly that of Alan Morgan, Charles Chan, and Naomi Shiboaka of the polarized target group. This experiment would not have been possible without their help and involvement. This project was supported by grants from the National Science and Engineering Council of Canada and the U.S. Department of Energy.

<sup>1</sup>U. Wiedner, K. Göring, J. Jaki, U. Klein, W. Kluge, H. Matthäy, E. Pedroni, W. Fetscher, H. J. Gerber, and R. Koch, Phys. Rev. Lett. **58**, 648 (1987).

<sup>2</sup>J. T. Brack *et al.*, Phys. Rev. C **34**, 1771 (1986).

<sup>3</sup>J. T. Brack, J. J. Kraushaar, D. J. Rilett, R. A. Ristinen, D. F. Ottewell, G. R. Smith, R. G. Jeppesen, and N. R. Stevenson, Phys. Rev. C **38**, 2427 (1988).

<sup>4</sup>C. Amsler, F. Rudolf, P. Weymuth, L. Dubal, G. H. Eaton, R. Frosch, S. Mango, and F. Požar, Phys. Lett. **57B**, 289 (1975).

<sup>5</sup>C. Amsler, L. Dubal, G. H. Eaton, R. Frosch, S. Mango, F.

Požar, and U. Rohrer, Lett. Nuovo Cimento **15**, 209 (1976).

<sup>6</sup>J. C. Alder *et al.*, Phys. Rev. D **27**, 1040 (1983).

<sup>7</sup>W. Gorn, C. C. Morehouse, T. Powell, P. R. Robrish, S. Rock, S. Shannon, H. M. Steiner, and H. Weisberg, Bull. Am. Phys. Soc. **12**, 469 (1967); J. F. Arens, O. Chamberlain, H. E. Dost, M. J. Hansroul, L. E. Holloway, C. H. Johnson, C. H. Schultz, G. Shapiro, H. M. Steiner, and D. M. Weldon, Phys. Rev. **167**, 1261 (1968).

<sup>8</sup>G. R. Smith, E. L. Mathie, E. T. Boschitz, C. R. Otterman, S. Mango, J. A. Konter, M. Daum, M. Meyer, R. Olszewski,

- and F. Volger, *Phys. Rev. C* **29**, 2206 (1984).
- <sup>9</sup>G. R. Smith *et al.*, *Phys. Rev. Lett.* **57**, 803 (1986).
- <sup>10</sup>G. R. Smith *et al.*, *Phys. Rev. C* **38**, 240 (1988).
- <sup>11</sup>G. Wait *et al.*, *Nucl. Instrum. Methods* **A274**, 515 (1989).
- <sup>12</sup>TRIUMF Users' Handbook (unpublished).
- <sup>13</sup>R. A. Arndt and L. O. Roper, SAID Phase Shift Analysis Program.
- <sup>14</sup>B. K. Jennings, *Phys. Lett. B* **205**, 187 (1988); B. K. Jennings and A. S. Rinat, *Nucl. Phys.* **A485**, 421 (1988).